# Preliminary estimation of fat depth in the lamb short loin using a hyperspectral camera

*S. Rahman[A], P. Quin[A,D], T. Walsh[A], T. Vidal-Calleja[A], M.J. McPhee[B], E. Toohey[C], and A. Alempijevic[A]*

[A]Center for Autonomous Systems, University of Technology Sydney

[B]NSW Department of Primary Industries, Livestock Industries Centre, Armidale, NSW 2351, Australia

[C]NSW Department of Primary Industries, PO Box 865, Dubbo, NSW 2830, Australia

[D]Corresponding author: Email: phillip.quin@uts.edu.au

**Running head:** Preliminary estimation of fat depth in the lamb short loin

**Abstract.** The objectives of this study were to describe the approach used for classifying surface tissue, and for estimating fat depth in lamb short loins and validating the approach. Fat versus non-fat pixels were classified and then used to estimate the fat depth for each pixel in the hyperspectral image. Estimated reflectance, instead of image intensity or radiance, was used as the input feature for classification. The relationship between reflectance and the fat/non-fat classification label was learnt using Support Vector Machines. Gaussian Processes were used to learn regression for fat depth as a function of reflectance. Data to train and test the machine learning algorithms was collected by scanning 14 short loins. The hyperspectral camera captured lines of data of the side of the short loin (i.e. with the subcutaneous fat facing the camera). Advanced Single Lens Reflex camera took photos of the same cuts from above, such that a ground truth of fat depth could be semi-automatically extracted and associated with the hyperspectral data. A subset of the data was used to train the machine learning model, and to test it. The results of classifying pixels as either fat or non-fat achieved a 96% accuracy. Fat depths of up to 12mm were estimated with

0.85 $R^2$, a mean absolute bias of 0.42mm and 0.8mm root mean square error. The techniques developed and validated in this study will be used to estimate fat coverage to predict total fat, and subsequently lean meat yield in the carcass.

**Additional keywords:** meat composition, lamb processing, hyperspectral imaging

## Introduction

Assessing the composition and quality of beef and sheep carcasses is important feedback for both the producer and the abattoir. Not only do abattoirs adhere to strict food health and quality standards, but carcasses must also meet specifications for export to particular markets. Knowing the carcass composition, the amount of fat (i.e., the fat score or fat depth), and therefore having an estimate of the lean meat yield (LMY) of a carcass can aid in improving abattoir efficiency and generating the highest return (Anon 2005). Producers also benefit from accurate estimates of carcass composition, as this objective carcass data can be used to help monitor and improve genetic performance and potentially optimise future animal nutrition plans prior to slaughter.

This paper assesses the possibility of using a near-infrared (NIR) hyperspectral camera to develop a non-destructive technique which classifies carcass surface regions of interest as either fat or muscle, and further, predicts fat depth in mm, without requiring trained assessors. The most precise non-destructive method for estimating carcass composition is computer tomography (CT) (Kongsro et al. 2009), but CT scanning is time consuming and expensive. Instead, current carcass fat depth is determined either via a subjective assessment where a fat score of 1-5 is allocated (with 1 the leanest and 5 the fattest) or by an objective measure of GR (total tissue depth at the twelfth rib 110mm from the midline) (Anon 2005). The latter measure of fat normally applies to carcasses sold over the hooks and is measured using a GR knife. A similar approach is taken in different EU countries including the UK where a carcass weight is recorded and a subjective score is allocated for fatness and conformation (Lambe *et al.* 2009). However, the accuracy of LMY prediction using hot carcass weight and GR tissue depth is variable, due to measurement error by assessors and genetic differences in animals (Siddell *et al.* 2012; Williams et al. 2017). Devices to predict the overall LMY that exploit RGB camera data such as VIASCAN (Cannell *et al.* 1999) have been developed with mixed prediction capability and commercial success. More recently, devices to predict proportions of bone, muscle and fat of the overall carcass or section thereof, based on dual X-ray absorptiometer (DEXA) systems are being developed with increasing prediction precision (Graham *et al.* 2015). While GR is a point measurement and DEXA is an overall carcass measurement, leverage can be made of the relationship between subcutaneous fat and total fat distributed through the carcass (Kempster 1995) if subcutaneous fat depth can be estimated reliably.

Hyperspectral capture high-dimensional data and are used in many food quality assessment scenarios (Huang *et al.* 2014). Hyperspectral cameras can be used, for example, to estimate meat tenderness (Naganathan et al. 2008; Saadatian et al. 2015) or the fat composition in atlantic salmon (Zhu *et al.* 2014). To the best of our knowledge, hyperspectral cameras have not been used to estimate fat depth. In our method to estimate fat depth, reflectance of fat and muscle is estimated from hyperspectral images by following the approach taken by (Huynh and Robles-Kelly 2010). These reflectance values are used by a Support Vector Machine (SVM) (Burges 1998) to classify surface tissue, Since SVMs have previously generated good classification results of materials from hyperspectral data (Garc´ıa Allende 2008). Principal component analysis and Gaussian processes (Rasmussen and Williams 2006) are used to perform regression on fat depth, since good results have been achieved even on high dimensional data, such as from a hyperspectral camera (Chen *et al.* 2007).

The objectives of this study were to: (1) describe the approach used for classifying surface tissue, and for estimating fat depth and (2) validate the approach.

## Materials and methods

This section presents the approach for estimating the depth of subcutaneous fat at each point of the surface of a meat sample: the acquisition of hyperspectral data, the determination of ground truth for fat depth, classification between fat and non-fat surfaces, and the training of the fat depth model.

### *Data*

The meat specimens used for training and testing the models in this study were derived from lamb short loin (Anon , 2005) cut to approximately 15-20mm thick. In total 11 samples were used exhibiting a range of subcutaneous fat thicknesses. Specimens were stored in a fridge at $3^{\circ}$ C except while being imaged in a room at ambient temperature.

*Acquiring Hyperspectral and Ground Truth Data*

The hyperspectral camera used was a Resonon Pika NR line scanner, the hyperspectral images have a spatial dimension of 320pixels in the line, each pixel has 146 bands in the range of $[954 - 1677]$ nm in 4:9 nm gaps. The specimen was placed on a platform which moved up or down at constant speed along a rail at a fixed distance from the camera to which the camera had been focused, so that a composite hyperspectral image of the entire side on view of the short loin could be created. The resulting hyperspectral image from the scanning process of each specimen has a spatial dimension of $320 \times 100$ pixels and 146 bands. Two 500W halogen lights were placed above and to the side of the hyperspectral camera to illuminate the sample. Each specimen was captured twice with only one of the two light sources turned on. The full experimental setup can be seen in Fig. 1.

[Fig. 1 about here.]

A Digital Single Lens Reflex (DSLR) camera was affixed to a tripod such that images of the short loins could be taken from above, as shown in Fig. 2 orthogonally to the viewing direction of the hyperspectral camera. From these images, the thickness of fat along the viewing axis of the hyperspectral camera could be determined in a semi-autonomous fashion, using the colour difference between fat and muscle.

[Fig. 2 about here.]

A laminated wooden calibration object placed on the platform, shown in Fig. 3, viewed by both the hyperspectral camera and the DSLR camera, allowed for establishing a relationship between fat depth measurements and pixels in the hyperspectral images via the relationship between pixels in the DSLR camera image and fat depth. The ground truth of fat depth in mm, including fat depths of 0 when no fat was present, was obtained for each pixel of the short loin, assuming that the fat depth was consistent through the thickness of the short loin sample.

[Fig. 3 about here.]

*Estimating Reflectance*

Reflectance, being a unique photometric property of an object, provides discriminative information about the object and is invariant to changes in illumination directions, illumination power spectra, and object shapes. For these reasons, we build our model based on this feature to classify fat vs. non-fat pixels, and to estimate fat depth.

Unlike radiance, reflectance, cannot be directly obtained from an image. Since object shape, reflectance, and illumination coexist and collectively compose an image of a scene, recovery of reflectance requires the separation and recovery of these geometric and photometric factors. From a computational perspective, estimating the photometric and geometric properties from a single input image is an under-constrained problem. To render the problem well posed, several approaches (Huynh and Robles-Kelly 2010; Rahman and Robles-Kelly 2013) utilise the information-rich representation of hyperspectral image and cast the recovery problem in a structural optimisation setting.

We start by mathematically describing the scene using the dichromatic reflectance model introduced by Shafer (1985), where the total surface radiance is considered the sum of two independent reflection components, namely specular and diffuse. Let an object with surface radiance $I(u, \lambda)$ at pixel-location $u$ and wavelength $\lambda$ be illuminated by an illuminant whose spectrum is $L(\lambda)$, the spectral radiance is given by:

$$I(u,\lambda) \; = \; g(u)L(\lambda)S(u,\lambda) \; + \; k(u)L(\lambda) \qquad (1)$$

The first term in the right-hand side of the above equation describes the diffuse reflection component, where $g(u)$ denotes the shading factor (i.e. the angle between the incoming light direction and surface normals), $L(\lambda)$ stands for the light spectrum and $S(u, \lambda)$ is the spectral reflectance. The second term in the right-hand side corresponds to the specular component, where $k(u)$ models specular coefficients of the scene.

Using this model, we aim to recover reflectance along with other model parameters from the spectral radiance of the image. To this end, we apply the approach described in (Huynh and Robles-Kelly 2010) and cast the estimation problem as minimising a cost function through iterative recovery of the reflectance model parameters.

The cost function $C(\Im)$, as given in Equation 2, is formed as the weighted sum of the dichromatic error, i.e. the squared difference between the observed data and the estimated yielded by the dichromatic model and a regularisation term $R(u)$.

$$C(\Im) \triangleq \sum_{u\in\Im}\left[\sum_{\lambda\in W}\left[I(u,\lambda) - \big(g(u)S(u,\lambda) + k(u)\big)L(\lambda)\right]^2 + \alpha R(u)\right] \qquad (2)$$

where $\Im$ is the image spatial domain and $W$ is the wavelength range. $\alpha$ is a constant that acts as a balancing factor between the dichromatic error and the regularisation term.

Next, we employ a coordinate descent approach (Boyd and Vandenberghe 2004) to recover the reflectance model parameters which yield the minimum of the cost function in Equation 3. The algorithm comprises two interleaved minimisation steps. At each iteration it solves for $L$ and the triplet $g(u)$, $S(u, \lambda)$, $k(u)$ in separate steps. Once it estimates one parameter, the optimal value of that is used to obtain the latter ones. Thus the optimisation iterates between these two steps until convergence is reached. Note that, the algorithm assumes convergence when none of the parameters change by an amount beyond a threshold between two successive iterations. From here on, the reflectance recovered based on the physics-based model is referred to as 'estimated reflectance'.

Some of the existing hyperspectral image based approaches also utilise reflectance to build their prediction models, e.g. to determine beef tenderness (Naganathan *et al.* 2008; Saadatian *et al.* 2015) or fat composition in atlantic salmon (Zhu *et al.* 2014). However, these approaches compute reflectance by applying spectral calibration, i.e. normalising raw radiance by illumination spectra. The illumination spectra is usually determined by taking hyperspectral image of a white reflection standard (e.g. Spectralon or sheets of white Teflon) which is assumed to be 100% reflective at all wavelengths .

As reported by Huynh and Robles-Kelly (2010) and Rahman and Robles-Kelly (2013) reflectance acquired by calibration, hereafter referred to as 'calibrated reflectance', is not robust to photometric changes and cannot provide results as accurate as those yielded by reflectance estimated by the physics based reflectance model. To further confirm results based on estimated reflectance are compared against that yielded by the calibrated reflectance.

*Classifying Fat*

Classifying between fat and non-fat (i.e, muscle) pixels in a composite hyperspectral image was done using a Support Vector Machine (SVM) with a Radial Basis Function (RBF) kernel (Vert et al. 2004). Support Vector Machines are supervised learning models based on kernel methods commonly applied to classification problems (Burges 1998). A basic SVM predicts, for each given input, which of two possible classes forms the output, making it a non-probabilistic binary classifier in its simplest form. Given a training set, the SVM training algorithm builds a model that assigns new examples into one category or the other. A SVM model is therefore a representation of the examples as points in space, mapped so that the examples of the separate categories are divided by a clear gap that is as wide as possible. New examples (testing set) are then mapped into that same space and predicted to belong to a category based on which side of the gap they fall on. An example of the SVM classification results for one short loin sample can be seen in Fig. 4

[Fig. 4 about here.]

*Estimating Fat Depth*

A Gaussian Process (GP) model (Rasmussen and Williams 2006) was trained with reflectance feature and measured fat depth (from the DSLR image) per pixel of the hyperspectral composite images. A Matérn kernel was used for this application. Gaussian Process models are other type of supervised learning models based on kernel methods, but in this case, commonly applied to regression problems. GPs can be seen as a distribution over functions. The method assumes that a set of random variables are jointly distributed. The main idea is that if the random variables are deemed by the kernel to be similar, then the output of the function at those points is expected to be similar too. Given a training set, GP learning algorithm builds a continuous stochastic model. The model can later be query at any input point and produce an estimated value with uncertainty based on how close the queried point is to the training data.

Having learnt the GP regression model, fat depth could be estimated per pixel of the hyperspectral composite image. An example of fat depth estimation on a short loin is shown in Fig. 5; the same short loin as shown in Fig. 2 and 4.

[Fig. 5 about here.]

## Results

To evaluate our method, we compare our results against ground truth and those yielded by using the alternative feature, the calibrated reflectance.

*Classification of fat vs. non-fat*

The data set for classification was made up of 22 hyperspectral images. To obtain the training data-set, 34,914 fat pixels and 18,346 non-fat pixels were selected from several regions of the input images. Subsequently, two features, i.e. estimated reflectance and calibrated reflectance, were extracted from the training set and used as input to a SVM classifier. To classify fat versus non-fat pixels, the resulting SVM model was applied to the rest of the pixels in the data set.

Fig. 4 presents a qualitative illustration of classification on a sample lamb chop, obtained using two variants of the reflectance feature. From left to right in Fig. 4, we show the hyperspectral input image, a sample training image with labelled fat regions (blue), and non-fat regions (red), classification of fat vs. non-fat pixels using the estimated reflectance, and the calibrated reflectance . Further, from Fig. 4, we can see that the estimated reflectance yields more visually accurate fat and non-fat separation than the alternative feature. This is evident in regions where pixels in the muscle and background are falsely classified as fat pixels

We also compare the two classification schemes in Table 1 of classification} in terms of classification rate (CR), correct detection rate (CDR) and false detection rate (FDR). Here, CR presents the total percentage of fat and non-fat pixels classified accurately, CDR stands for the percentage of fat pixels correctly classified and, FDR corresponds to the percentage of non-fat pixels falsely classified as fat. Note that, CDR, FDR, and CR have been computed by comparing our results against the ground truth data, which has been obtained by manually labelling fat and non-fat pixels for all images in the data set. As expected, the estimated reflectance delivered more accurate results than the calibrated reflectance, which is consistent with the qualitative results presented above.}

The poor classification results obtained by calibrated reflectance can be explained by the variation induced by the illuminant spectrum and the surface shading. Since normalising radiance by illuminant power does not achieve surface shading-independence and disregards the specular components inherent to the dichromatic model, calibrated reflectance cannot yield as accurate result as the estimated reflectance when the shape, illumination direction or power spectra change between the training and testing images.

[Table 1 about here.]

*Estimation of fat depth*

The data set for fat depth estimation included 5,317 pixels (2779 and 3223 respectively with the light sources) visible in both the composite hyperspectral camera view and the DSLR camera view, and therefore for which ground truth depth was known. The GP was trained on data acquired by one light source and tested with data acquired with the other light source.

We compare our result of fat depth against the ground truth values and, that obtained using the calibrated reflectance. To this end, Fig. 5 presents qualitative results of the capacity of our method to recover fat depth of an example short loin. From left to right in the figure, we show a top down view of the sample captured by a DSLR camera with labelled fat regions under study, ground truth fat depth as measured from the DSLR image and predicted fat depth by using the estimated reflectance and calibrated reflectance.

Fig. 6 presents a comparison of actual vs. predicted depth values as yielded by GP when trained to learn regression as a function of either of the features, calibrated reflectance or estimated reflectance, in Fig. 6a. and Fig. 6b respectively. We also provide quantitative results in Table 2.

[Fig. 6 about here.]

[Table 2 about here.]

Analysing both the qualitative and quantitative results, we can conclude that though there is a strong correlation between the models predictions and actual results while trained using either of the feature, the estimation was more accurate for the estimated reflectance.

## Discussion and Conclusions

Saleable meat yield is a function of the weight of muscle relative to the weight of the carcass, and represents a key determinant of carcass value along the supply chain. Therefore, most Australian processors offer price grids that take account of both carcass weight and fatness. Currently a single point measure at the GR site acts as a surrogate to estimate whole body fatness. More recently, devices to predict proportions of bone, muscle and fat of the overall carcass based on DEXA systems have been deployed. While GR is a point measurement and DEXA is an overall carcass measurement, leverage could be made of the relationship between subcutaneous fat and total fat distributed through the carcass. While traditional approaches of video image analysis use RGB cameras for overall fat estimation, this paper presents an approach to subcutaneous fat estimation using a hyperspectral imaging. The inherent advantage of hyperspectral cameras is they capture the light spectrum range where materials exhibit specific reflectance or absorption features related to material composition and variability.

Classification of fat vs. non-fat regions, and estimation of fat depth in mm was accomplished using Near-Infrared hyperspectral imaging. This paper demonstrated accurate classification of fat and non-fat regions using a SVM (96.27% correct classification), and accurate estimation of fat depth using a Gaussian Process model ($R^2$ = 0.85). Results demonstrate the estimation to be more accurate using the robust dichromatic physics based model of reflectance rather than the traditional normalised reflectance model.

In future work, we intend to increase the size of the training and testing sets, to ensure that this method generalises to a larger population and variety of animals. Collecting data from a full carcass, rather than short loin portions, will also allow for a greater variety of fat depths, angles of incidence, and lighting.

**Acknowledgments**

This paper is supported by funding from the Australian Government Department of Agriculture and Water Resources as part of its Rural R&D for Profit programme.

**References**

Anon (2005) Handbook of Australian Meat 7th Edition (International Red Meat Manual).

Boyd S, Vandenberghe L (2004) 'Convex optimization.' (Cambridge university press: United Kingdom)

Burges CJ (1998) A tutorial on support vector machines for pattern recognition. *Data mining and knowledge discovery* **2**, 121–167.

Cannell, R. C., Tatum, J. D., Belk, K. E., Wise, J. W., Clayton, R. P., & Smith, G. C. (1999). Dual-component video image analysis system (VIASCAN) as a predictor of beef carcass red meat yield percentage and for augmenting application of USDA yield grades. *Journal of animal science*, 77(11), 2942-2950.

Chen T, Morris J, Martin EL (2007) Gaussian process regression for multivariate spectroscopic calibration. *Chemometrics and Intelligent Laboratory Systems* **87**, 59-71.

Gardner G, Glendenning R, Brumby O, Starling S, William A (2015). The development and calibration of a dual X-ray absorptiometer for estimating carcass composition at abattoir chain-speed. in Fourth Annual Conference on Body and Carcass Evaluation, Meat Quality, Software and Traceability, At Edinburgh, Scotland, Garc´ıa Allende PB, Anabitarte Garc´ıa F, Conde Portilla OM, Mirapeix Serrano JM, Madruga Saavedra FJ, Lo´pez Higuera JM (2008) Support vector machines in hyperspectral imaging spectroscopy with application to material identification. In 'SPIE Society of Photo-Optical Instrumentation Engineers.

Huang H, Liu L, Ngadi M (2014) Recent developments in hyperspectral imaging for assessment of food quality and safety. *Sensors* **14**, 72487276.

Huynh CP, Robles-Kelly A (2010) A solution of the dichromatic model for multispectral photometric invariance. *International Journal of Computer Vision* **90**, 1-27.

Kempster A.J. (1981), Fat partition and distribution in the carcasses of cattle, sheep and pigs: A review, *Meat Science*, **5**, 83-98,

Kongsro J, Røe M, Kvaal K, Aastveit AH, Egelandsdal B (2009) Prediction of fat, muscle and value in Norwegian lamb carcasses using EUROP classification, carcass shape and length measurements, visible light reflectance and computer tomography (CT). *Meat Science* **81**, 102-107.

Lambe NR, Navajas EA, Bünger L, Fisher AV, Roehe R, Simm G (2009) Prediction of lamb carcass composition and meat quality using combinations of post-mortem measurements. *Meat Science* **81**, 711-719.

Naganathan GK, Grimes LM, Subbiah J, Calkins CR, Samal A, Meyer GE (2008) Visible/near-infrared hyperspectral imaging for beef tenderness prediction. *Computers and Electronics in Agriculture* **64**, 225-233.

Rahman S, Robles-Kelly A (2013) An optimisation approach to the recovery of reflection parameters from a single hyperspectral image. *Computer Vision and Image Understanding* **117**, 1672-1688.

Rasmussen CE, Williams C (2006) ' Gaussian Processes for Machine Learning.' ( MIT Press: Cambridge, MA, USA)

Saadatian F, Liu L, Ngadi MO (2015) Hyperspectral imaging for beef tenderness assessment. *International Journal of Food Processing Technology* **2**, 18–25.

Shafer SA (1985) Using color to separate reflection components. *Color Research & Application* **10**, 210-218.

Siddell J, McLeod BM, Toohey ES, van de Ven R, Hopkins DL (2012) The prediction of meat yield in lamb carcasses using primal cut weights, carcass measures and the Hennessy Grading Probe. *Animal Production Science* **52**, 584-590.

Vert JP, Tsuda K, Scho¨lkopf B (2004) A primer on kernel methods. In 'Kernel Methods in Computational Biology.' pp. 35–70.

Williams A, Anderson F, Siddell J, Pethick DW, Hocking Edwards JE, Gardner GE (2017) Predicting lamb carcase composition from carcase weight and gr tissue depth. In 'International Congress of Meat Science and Technology. pp. 729–732.

Zhu F, Zhang H, Shao Y, He Y, Ngadi MO (2014) Mapping of fat and moisture distribution in atlantic salmon using near-infrared hyperspectral imaging. *Food and Bioprocess Technology* **7**, 1208–1214.

**Table 1: Accuracy of fat vs non-fat classification yielded by two different reflectance-based features as input for classification.**

| Error measure | Estimated reflectance | Calibrated reflectance |
|---|---|---|
| Classification rate % | 92.30±1.90 | 96.27±0.62 |
| Correct detection rate% | 90.39±1.85 | 93.28±1.46 |
| False detection rate % | 0.47±0.37 | 10.64±3.25 |

**Table 2: Statistics of estimating fat depth [mm] for the estimated and calibrated reflectance.**

| Error measure | Estimated reflectance | Calibrated reflectance |
|---|---|---|
| Correlation coefficient $R^2$ | 0.85 | 0.79 |
| Mean absolute error | 0.42 | 0.65 |
| Root mean square error | 0.80 | 0.99 |

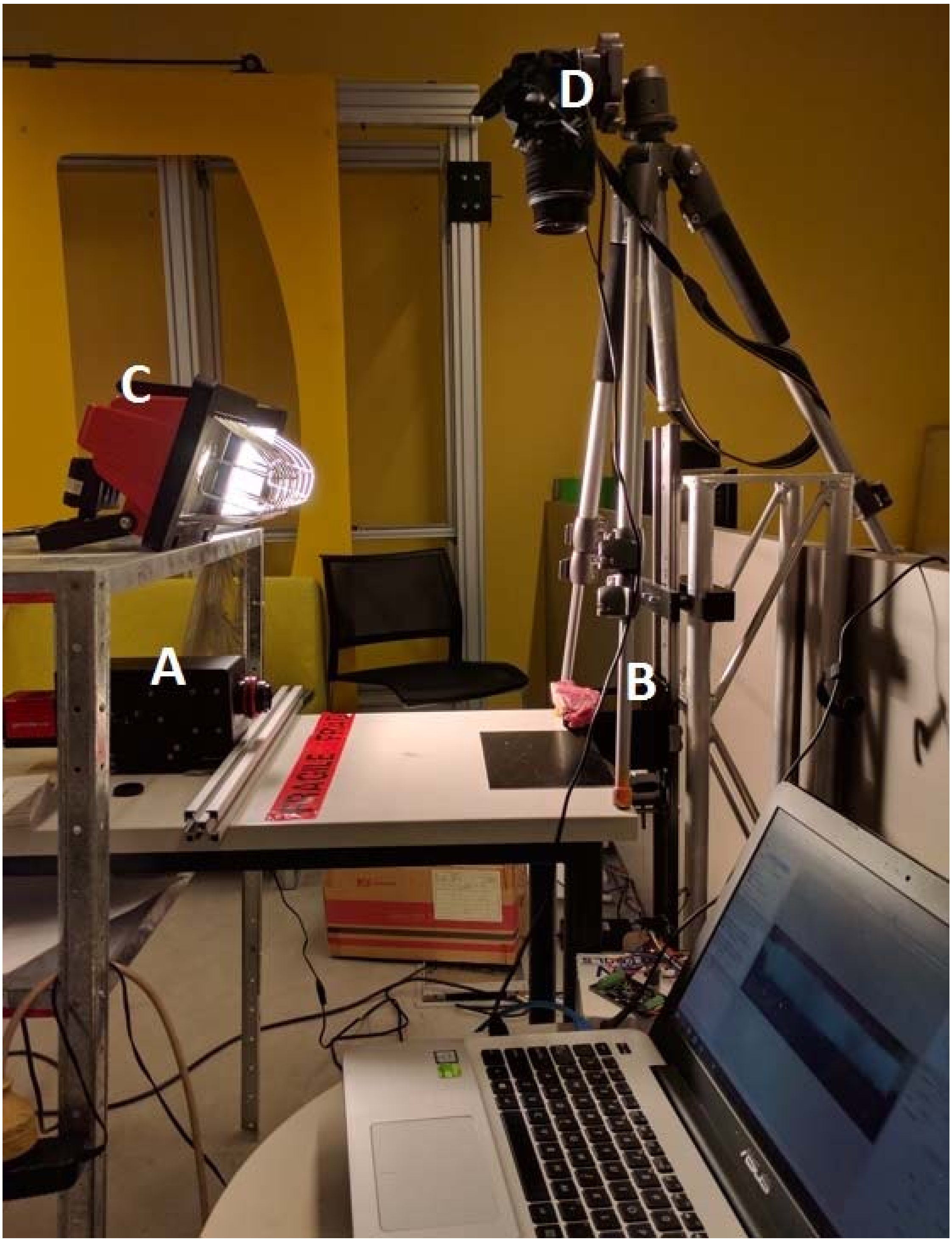


Fig. 1: The experimental setup showing: A) the hyperspectral camera, B) the short loin on the rail platform, C) the halogen light, D) the Digital Single Lens Reflex camera.

Fig. 2: An example short loin specimen placed on the platform, photographed from above by the Digital Single Lens Reflex camera.

(a) (b)

Fig. 3: The calibration object. (a) Black dots on the left side of the object's topmost surface are visible as lines to the hyperspectral camera. The grid is viewable to the Digital Single Lens Reflex camera. (b) Dots become lines in the hyperspectral image when wavelengths are the vertical dimension of the image.

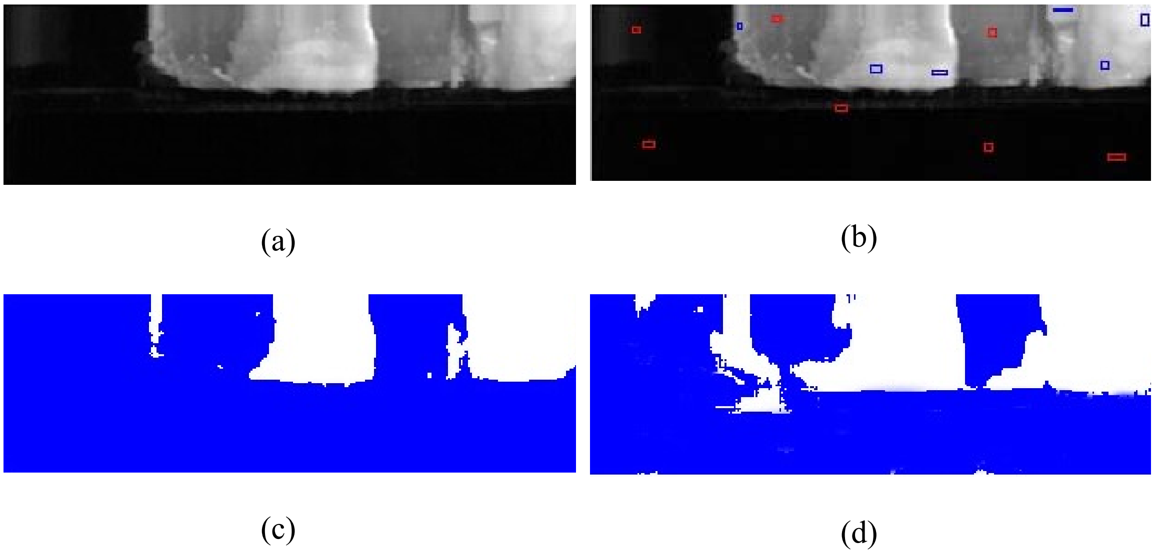


Fig. 4: A qualitative illustration of the capacity of our method to classify fat vs non-fat pixels in a sample lamb chop. (a) Hyperspectral image of the sample captured at 1447 nm. (b) A sample training image with labelled fat regions (with blue borders) and non-fat regions (with red borders). Separation of fat (white pixels) vs. non-fat (blue pixels) regions by using (c) estimated reflectance and (d) calibrated reflectance as feature for classification.

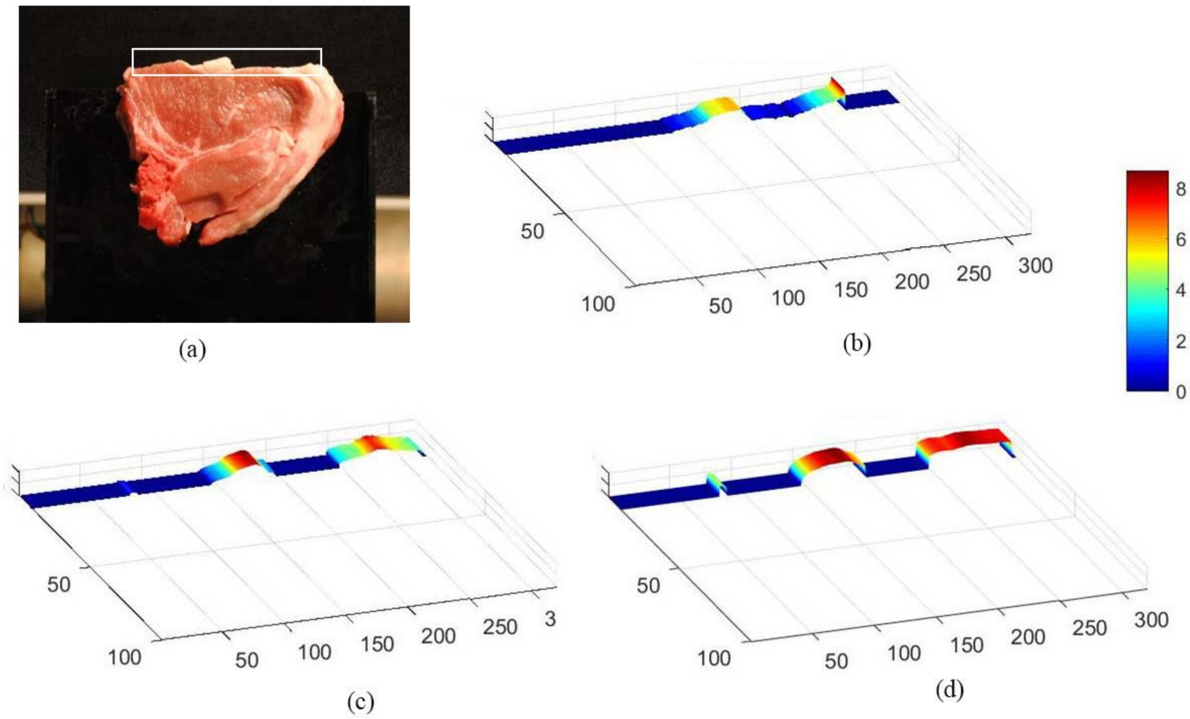


Fig. 5: A qualitative illustration of the capacity of our method to recover fat depth of an example short loin. From left to right: (a) Top down view of the sample captured by a DSLR camera with labelled fat regions under study. (b) Ground truth fat depth as measured from the DSLR image. Predicted fat depth by using the (c) estimated reflectance and, (d) calibrated reflectance.

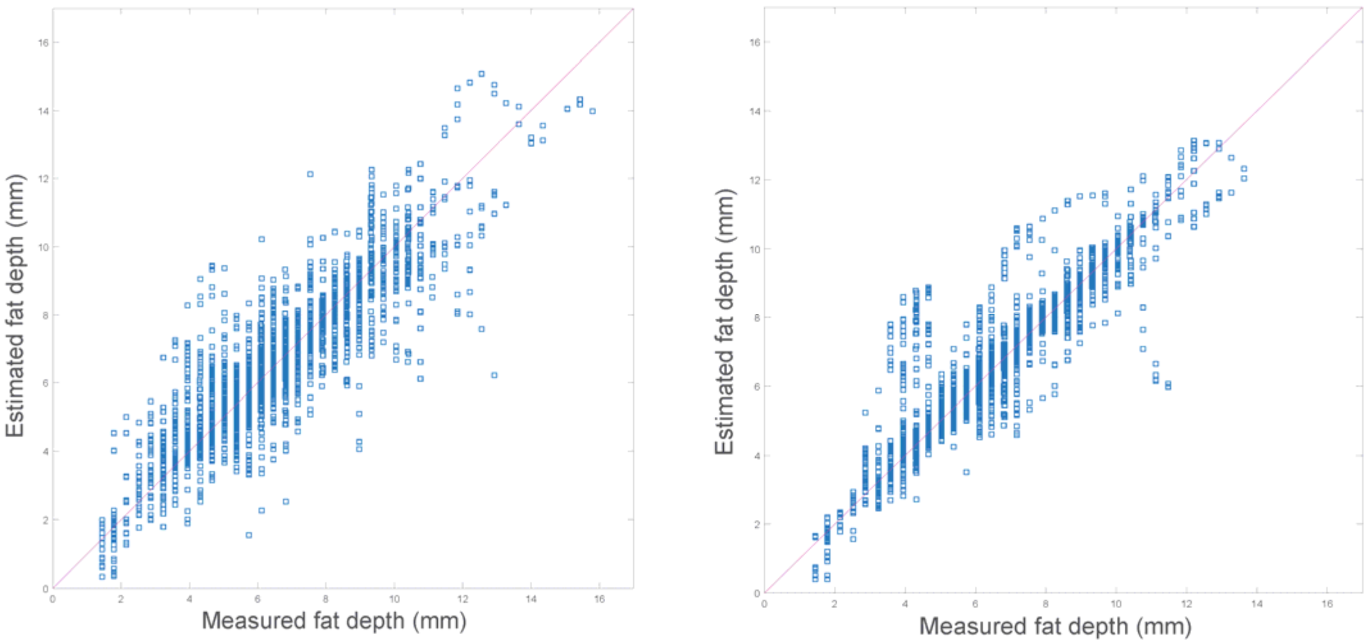


(a) (b)

Fig. 6: Results of fat depth estimation based on the Gaussian Process model vs. ground truth fat depth in mm. (a) Using calibrated reflectance as the feature (b) Using the estimated reflectance as the feature